A New Photocatalyst Bismuth Oxo Citrate: Synthesis, Characterization, and Photocatalytic Performance

Slobodan M. Najdanović[1*], Milica M. Petrović[1], Ian J. Slipper[2], Miloš M. Kostić[1], Marija D. Prekajski[3], Jelena Z. Mitrović[1], Aleksandar Lj. Bojić[1]

ABSTRACT: A new photocatalyst bismuth oxo citrate was synthesized by facile precipitation process with calcination at 200 °C. The photocatalyst was characterized by scanning electron microscopy (SEM), X-ray diffraction (XRD), Fourier-transform infrared (FTIR) spectroscopy, N_2 sorptometry, and elemental analysis. Morphologically, it is composed of polyhedral particles with different, irregular shapes and sizes. The specific surface area (SSA) of the photocatalyst was 8.92 $m^2\ g^{-1}$. It showed very good photocatalytic performance and reusability. Total decolorization of Reactive Blue 19 (RB19) was achieved in less than 10 minutes, which is much faster in comparison with TiO_2 P25. Also, bismuth oxo citrate showed higher photocatalytic activity than other photocatalysts based on bismuth compounds reported by other authors. Optimal photocatalysis parameters were pH 2 and photocatalyst dose of 250 mg dm^{-3}. The decolorization rate was found to decrease as initial dye concentration increased. The photocatalytic data best fitted to L–H kinetic model with pseudo-first order reaction rate. Chrastil diffusion model showed that diffusion has not influence on the process. *Water Environ. Res.*, **90** (2018).

KEYWORDS: bismuth oxo citrate, photocatalytic process, Reactive Blue 19, decolorization, kinetics.

doi:10.2175/WER-D-17-00201

Introduction

Wastewaters from dye production and application industries presents a serious threat to the environment (Xu et al., 2016). In the past 20 years, many treatments have been developed for water purification. Besides standard technologies, several new technologies, such as advanced oxidation processes (AOPs), have been developed (Xu et al., 2013). Among AOPs, heterogeneous photocatalytic processes, during which •OH radicals and other oxidative radicals are generated by using solar or artificial light illumination, are one of the most promising technologies for water purification (Kamat, 1993). The main advantage of heterogeneous photocatalysis is ability of the total mineralization of organic dyes, resulting in formation of CO_2, H_2O, and the corresponding mineral acids, leaving no waste for second disposal (Chen et al., 2010; Chong et al., 2010). Other advantages of heterogeneous photocatalysis are that it does not require using of any other chemicals or soluble catalysts, except insoluble photocatalyst, which can be recovered and re-used, so that secondary pollution is not formed.

In recent years, many contributors reported that photocatalysts based on bismuth compounds, such as Bi_2O_3, $BiVO_4$, Bi_2WO_6, BiOBr, BiOI, $Bi_6O_6(OH)_3(NO_3)_3 \cdot 1.5\ H_2O$, and $Bi_2O_2CO_3$, have high photocatalytic activity (Li et al., 2013; Li et al., 2014; Liang et al., 2016; Saison et al., 2011; Shang et al., 2009; Wang et al., 2016; Wu et al., 2013; Xie, Wang, Hu, Zheng et al., 2012).

To the authors' knowledge, photocatalytic properties of bismuth oxo citrate have never been investigated before. Bismuth-citrate (i.e., pharmaceutical products based on bismuth-citrate) is widely used in medicine for treating the diseases of the gastrointestinal tract, and it is the main component of pharmaceuticals for the treatment of infection by *Helicobacter pylori*, which causes gastric or duodenal ulcers (De-Nol, Lizhudele, Gist Brocades, Yamanouchi, GSK, Tritec, and Pylorid) (Yang and Sun, 2007). Bismuth (III) citrate is also used in the synthesis of bismuth containing high-temperature superconducting materials (Afonina et al., 2009).

[1] University of Niš, Faculty of Sciences and Mathematics, Department of Chemistry, Višegradska 33, 18000 Niš, Serbia.

[2] University of Greenwich at Medway, Faculty of Engineering and Science, Central Avenue, Chatham Maritime, Kent, ME4 4TB, England, UK.

[3] University of Belgrade, Institute of Nuclear Sciences, Materials Science Laboratory, 170 Vinča, P.O. Box 522, 11001 Belgrade, Serbia.

* University of Niš, Faculty of Sciences and Mathematics, Department of Chemistry, Višegradska 33, 18000 Niš, Serbia; Tel: +381 18 533 014; Fax: +381 18 533 014; e-mail: najda89@gmail.com.

The physical and chemical properties of the photocatalysts are strongly related to its synthesis method. It is very important to develop facile synthesis methods, which can produce bismuth oxo citrate with high photocatalytic performance. Among all the synthetic approaches for bismuth compounds, the precipitation method is the most commonly used in the industry, because it is simple and provide obtaining of high purity products (Afonina et al., 2009; Naydenko et al., 2012).

Therefore, the present study is focused on the synthesis of a new photocatalyst bismuth oxo citrate by the facile precipitation method and examination of its structure and photocatalytic activity. Characterization of photocatalyst was done by scanning electron microscopy (SEM), X-ray diffraction (XRD), Fourier-transform infrared (FTIR) spectroscopy, N_2 sorptometry, and elemental analysis. Also, its isoelectric point (pI) was determined. The photocatalytic activity was evaluated by decolorization of water solution of textile dye Reactive Blue 19 (RB19). In order to determine the optimal operating conditions, influence of parameters, such as initial pH, initial dye concentration, and initial photocatalyst dose, was investigated. Kinetics and diffusion models were examined for a better understanding of the photocatalytic process.

Experimental

Materials. All chemicals used in this study were of analytical grade and used without further purification. Bismuth (III) nitrate pentahydrate was purchased from Carlo Erba (Chech Republic), TiO_2 P25 (Aeroxide) from Evonik Industries (Canada), nitric acid, sodium hydroxide, sodium nitrate, Reactive Blue 19, Reactive Orange 4, Reactive Orange 16, citric acid, ethylene glycol, potassium bromide, and acetanilide from Sigma Aldrich (Germany). Deionized water was used in all experiments.

Synthesis of Photocatalyst. The bismuth oxo citrate photocatalyst was made by precipitation process using bismuth-nitrate pentahydrate [$Bi(NO_3)_3 \cdot 5\ H_2O$] as a precursor. One gram $Bi(NO_3)_3 \cdot 5\ H_2O$ was dissolved in a certain volume of diluted nitric acid and stirred to obtain a clear solution. Then, citric acid and ethylene glycol were added, pH was adjusted at 3.5 using sodium hydroxide, and the solution was magnetically stirred 3 hours until the precipitate was produced. The obtained precipitate of bismuth oxo citrate was rinsed several times with deionized water, centrifuged, and dried at 80 °C for 6 hours, and calcined in air at 200 °C for 1 hour at a heating rate of 15 °C min^{-1}. After that, the photocatalyst was cooled to room temperature and ready to use.

Characterization of Photocatalyst. The surface morphology of photocatalyst was observed using a JSM-5300 (JEOL, Peabody, Massachusetts, USA) scanning electron microscope (SEM) operating at 30 kV. A thin layer of gold was coated on the samples to increase conductivity and fixate tiny surface particles for better imaging. Phase composition was identified by X-ray diffraction (XRD) using powder X-ray diffractometer (Rigaku, Ultima IV, Japan). The XRD studies for all the powders were carried out with Cu Kα radiation (λ=1.5406 nm) produced at 40 kV and 40 mA. Experiments were performed in scan range 2θ=5-60° under 40 kV, 40 mA, with scan speed 5 degree min^{-1} and step size of 0.02 degree. Before measurement, the angular correction was done by high-quality Si standard. Fourier-transform infrared (FTIR) spectra were recorded in KBr dispersion in the range of 400 to 4000 cm^{-1} on BOMEM MB-100 (Hartmann & Braun, Canada) FTIR spectrometer. Nitrogen adsorption measurements were performed on a Gemini 5 Surface Area Analyser (Micromeritics, Norcross, Georgia, USA). Before the measurement, the samples were degassed under flowing nitrogen at 40 °C for 20 hours. The specific surface area was determined using the Brunauer–Emmett–Teller (BET) method (Brunauer et al., 1938). The Barret–Joyner–Halenda (BJH) method was used for pore volume, area, and diameter analysis (Barrett et al., 1951). Elemental analysis was performed with a 2400 Series II CHNS/O Elemental Analyzer (Perkin-Elmer, Waltham, Massachusetts, USA) with acetanilide as a standard. Carbon, nitrogen, and hydrogen contents were expressed as a percentage of dry weight. The isoelectric point of the photocatalyst was determined by the salt addition method (Mahmood et al., 2011). $NaNO_3$ solution (0.1 mol dm^{-3}) was used as inert electrolyte and series of test solutions were prepared by adjusting pH of 50 cm^3 of electrolyte in a range between 2 and 11 using 0.01 mol dm^{-3} HNO_3 and 0.01 mol dm^{-3} NaOH. Then, 0.2 g of photocatalyst was added to each solution, sealed and stirred for 24 hours. The final pH (pH_f) was measured after 24 hours and plotted against the initial pH (pH_i). The pI was taken as the point where pH_i=pH_f.

Determination of Photocatalytic Activity. The photocatalytic activity of the prepared photocatalyst was determined by decolorization of aqueous solution of RB19 at ambient temperature. All photochemical experiments were carried out in a batch photoreactor under UV light irradiation with light intensity of 1950 μW cm^{-2} and maximum emission at 253.7 nm (Mitrović et al., 2012). The pH of solutions was adjusted by adding NaOH or HNO_3, using pH-meter (SensIon5, HACH, Loveland, Colorado, USA). Appropriate amount of photocatalyst was added into 50 cm^3 dye solution, and solution was transferred to Petri dish and irradiated with UV light. During the decolorization experiments, the dye solutions were stirred on a magnetic stirrer. At the given time intervals about 4 cm^3 of suspension was collected, and then centrifuged and filtrated (MF, 0.45 μm) to remove the particles of photocatalyst. The concentration of RB19 was measured by a UV-Visible spectrophotometer (UV-1800, Shimadzu, Japan) by measuring absorbance at 592 nm. The decolorization efficiency (DE) was calculated using the following equation:

$$DE = \frac{c_0 - c_t}{c_0} \times 100 \quad (1)$$

where c_0 and c_t are the initial and final concentrations of the RB19 in the solution (mg dm^{-3}), respectively.

Results and Discussion

Characterization of Photocatalyst. *Scanning Electron Microscope Analysis*. The SEM images of the photocatalyst prepared by precipitation method are shown in Figure 1. The

Allen Press, Inc. ■ 5 April 2018 ■ 6:20 pm ■ Customer MS#WER-D-17-00201
//titan/Production/w/waer/live_jobs/waer-90/waer-90-07/waer-90-07-07/layouts/waer-90-07-07.3d

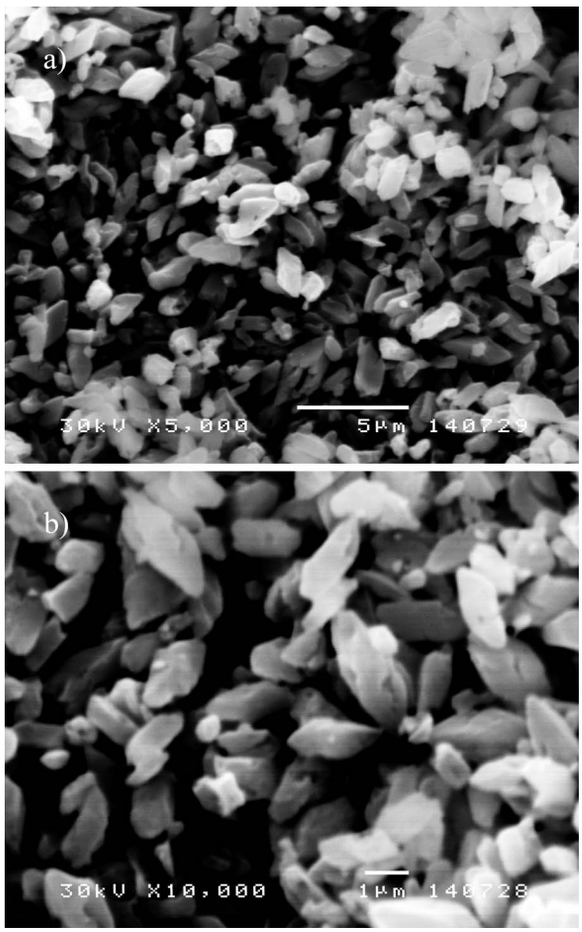

Figure 1—SEM images of bismuth oxo citrate photocatalyst.

material is composed of polyhedral particles with different, irregular shapes and sizes. Their lengths and thicknesses vary between approximately 0.5-3 μm and 0.3-1 μm, respectively. The obtained polyhedrons have apparently smooth surface, although the pores smaller than approximately 0.3 μm are observed in some polyhedrons. Some polyhedrons appear to be slightly sintered, and all this structure, overall, makes a relatively large surface area, which enables high photocatalytic activity of material.

Textural Properties. The specific surface area (SSA) has a significant influence on the photocatalytic performance, because the photocatalytic process mainly occurs at the surface of photocatalyst. With the increase of SSA, the number of active sites is greater and photocatalytic performance is enhanced (Li et al., 2013; Li et al., 2014). The N_2 adsorption/desorption isotherm of bismuth oxo citrate according to the IUPAC classification (Figure) belongs to type IV. A hysteresis loop indicates that this is a mesoporous material. The obtained SSA of photocatalyst using the BET method is 8.92 $m^2\ g^{-1}$. The value of SSA for bismuth oxo citrate is similar with other bismuth based photocatalyst reported in literature (Anandan et al., 2010; Irmawati et al., 2004; Li et al., 2013; Li et al., 2014; Liu et al., 2014; Shang et al., 2009; Xie, Wang, Hu, Zheng et al., 2012). The BJH method reveals that photocatalyst is mainly composed of mesoporous, presence of which has significant influence on enhanced photocatalytic performance of material. The BJH surface area of pores is 8.17 $m^2\ g^{-1}$, and volume of pores is 0.0327 $cm^3\ g^{-1}$. Average pore diameter is 16.03 nm.

X-Ray Diffraction Analysis. Results of XRD analysis, shown in Figure 2, indicate that the synthesized material is a bismuth oxo citrate $BiOC_6H_7O_7 \cdot H_2O$ that exhibits diffraction maxima with the *d* values equal to 10.26, 5.63, 4.64, 3.92, 3.37, and 2.11 Å as Naydenko et al. (2012) reported. Peaks are sharp and well defined, which indicates that the obtained bismuth oxo citrate is fully crystalline.

Fourier-Transform Infrared Spectroscopy Analysis. Fourier-transform infrared spectroscopy was done to detect the functional groups specific for bismuth oxo citrate, to confirm molecular structure of the photocatalyst. Presence of citrate in the form of bismuth oxo citrate salt can be proved by the bands in the FTIR spectrum of photocatalyst (Figure 3) at 1642 and 1536 cm^{-1}, which correspond to asymmetric stretching vibrations $\nu_{as}(COO^-)$ of carboxylate groups, and the bands at 1426 cm^{-1}, which correspond to the symmetrical vibrations $\nu_s(COO^-)$ of carboxylate groups (Naydenko et al., 2012). Absence of IR absorption bands above 1700 cm^{-1} indicates the absence of free –COOH groups, which means that the photocatalyst does not contain the free citric acid (Gyliene et al., 2007).

The FTIR spectrum shows broad absorption bands at 3437 and 3260 cm^{-1}, which correspond to the stretching modes of hydroxyl groups and lattice water. A band at 1623 cm^{-1} can be attributed to the banding vibrations modes of crystal water molecules (Evseenko et al., 2004; Lakshmanan, 1968).

The absorption bands in the range of 800 to 300 cm^{-1} can be attributed to the stretching modes of Bi–O bonds. The medium bands at 630, 561, 507, and 403 cm^{-1} are attributed to the Bi–O bond stretching vibration peaks (Fruth et al., 2004; Irmawati et al., 2004; Prekajski et al., 2010).

The weak bands in the region of 2993 to 2851 cm^{-1} originate from the asymmetric and symmetric stretches of the CH_2 groups. The corresponding deformation modes are between 1320 and 1360 cm^{-1} (Lakshmanan, 1968). The oscillations of the C–OH group are reflected by the bands in the region 1300 to 1070 cm^{-1} (Lakshmanan, 1968; Thottoli and Unni, 2013). The weak bands at 967, 947, and 927 cm^{-1} may be assigned to C–C stretching vibrations (Lakshmanan, 1968). The bands at 914, 850, and 837 cm^{-1} can be ascribed to the Cα–OH stretch (Taqa, 2011).

Elemental Analysis. Elemental analysis shows that bismuth oxo citrate photocatalyst is composed of 16.03% of C and 1.93% of H, which is in good agreement with theoretical values for $BiOC_6H_7O_7 \cdot H_2O$ (16.60% of C and 2.09% of H).

Based on the different structure analysis methods, it can be concluded that the photocatalyst is composed of bismuth oxo citrate, most likely in the form of $BiOC_6H_7O_7 \cdot H_2O$.

Isoelectric Point. The pI of the photocatalyst is 3.17 (Figure S2). That means that surface of the photocatalyst is acidic. At

Allen Press, Inc. ■ 5 April 2018 ■ 6:20 pm ■ Customer MS#WER-D-17-00201
//titan/Production/w/waer/live_jobs/waer-90/waer-90-07/waer-90-07-07/layouts/waer-90-07-07.3d

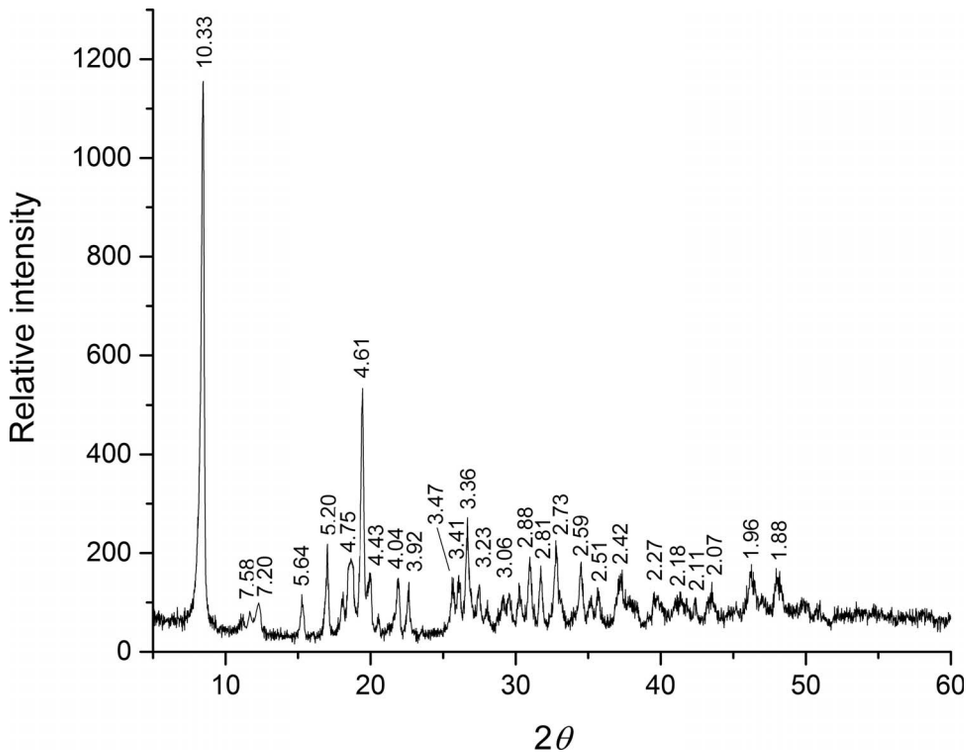

Figure 2—XRD pattern of bismuth oxo citrate photocatalyst.

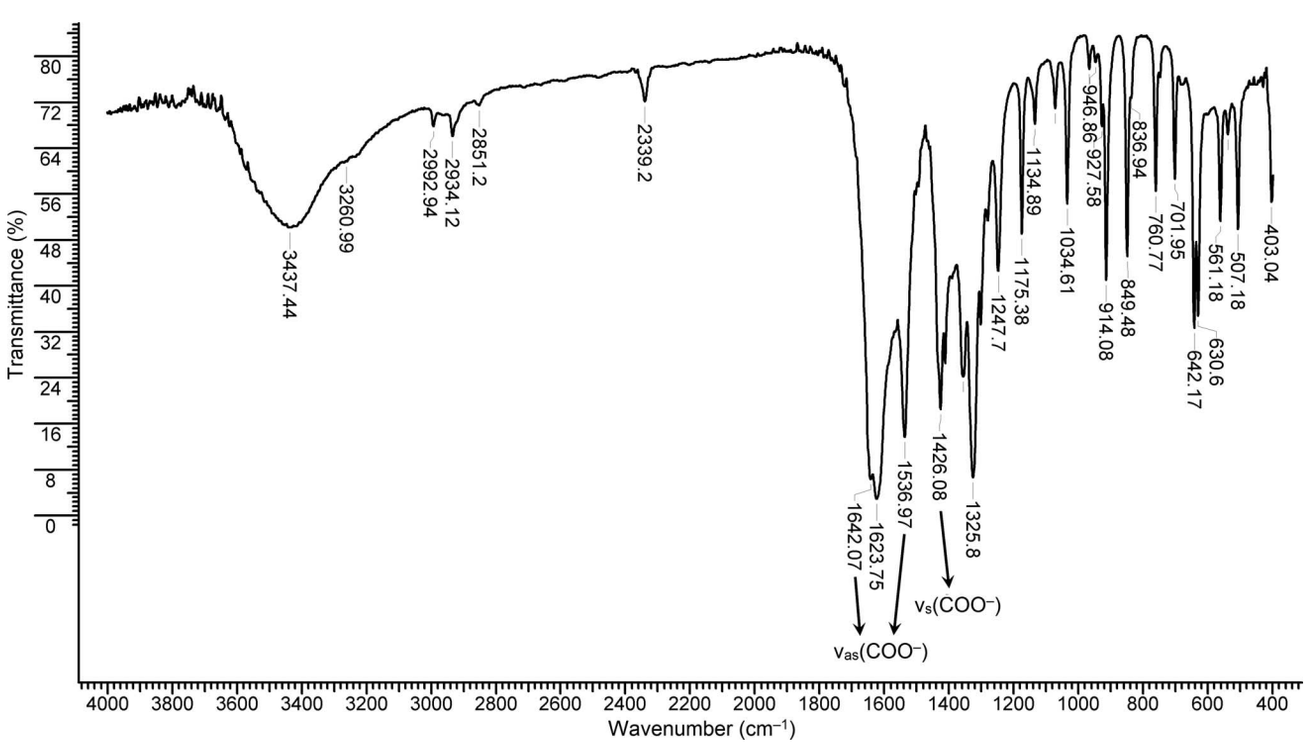

Figure 3—FTIR spectrum of bismuth oxo citrate photocatalyst.

Allen Press, Inc. ■ 5 April 2018 ■ 6:21 pm ■ Customer MS#WER-D-17-00201
//titan/Production/w/waer/live_jobs/waer-90/waer-90-07/waer-90-07-07/layouts/waer-90-07-07.3d

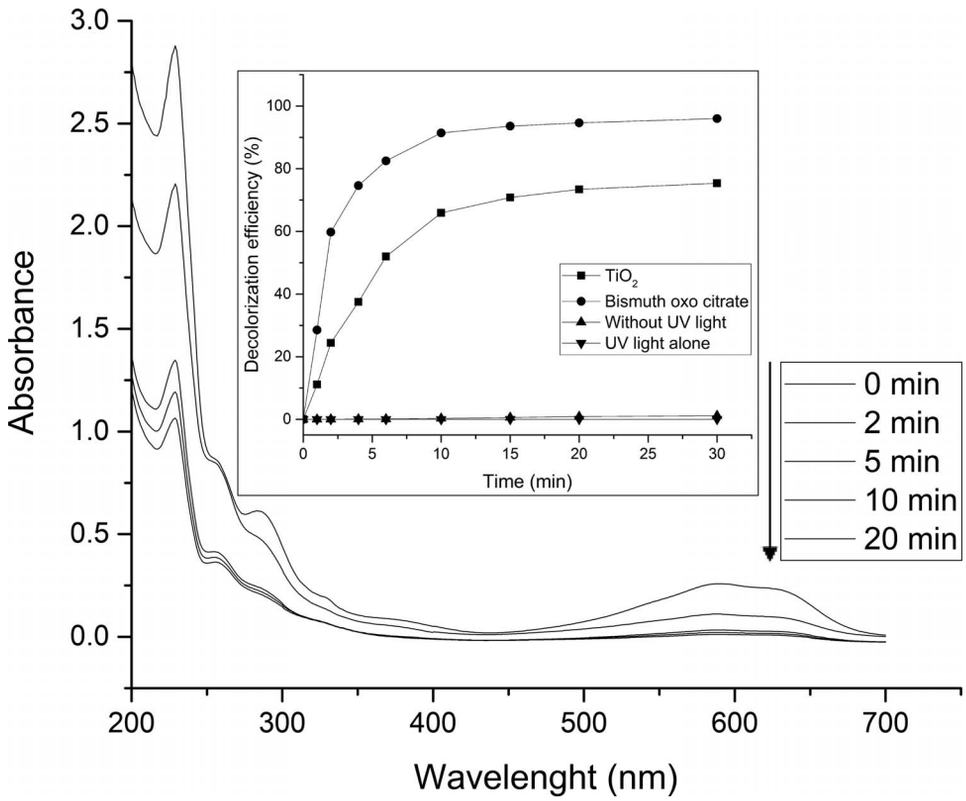

Figure 4—UV-Vis spectrum of RB19 during the photocatalytic process and decolorization efficiency of RB19. c_{RB19} 25 mg dm^{-3}, $c_{photocatalyst}$ 500 mg dm^{-3}, UV light intensity 1950 μW cm^{-2}, temperature 20.0 ± 0.5 °C, pH native (4.7).

pH lower than 3.17, its surface is positively charged, while it is negatively charged at pH higher than 3.17.

Photocatalytic Performance of the Synthesized Photocatalyst. Different experiments were done to determine the photocatalytic performance of bismuth oxo citrate photocatalyst and results are shown in Figure 4. The experiment without UV light showed that adsorption of RB19 on the photocatalyst is negligible. Under UV light radiation without adding of photocatalyst, the degradation of RB19 does not occurs. During the photocatalytic process, the absorption peaks of RB19 in visible and UV region rapidly decrease in time. The disappearance of peaks in UV region indicates that the photocatalytic process provides decomposition of the aromatic rings in RB19, which leads to complete degradation of dye. Total decolorization of dye (25 mg dm^{-3}) was achieved in less than 10 minutes. Therefore, it can be concluded that the photocatalyst based on bismuth oxo citrate shows high photocatalytic activity and it can be used for photocatalytic degradation of dye. To demonstrate high photocatalytic activity of bismuth oxo citrate, its photocatalytic activity was compared with well-known photocatalyst commercial TiO_2 P25 and photocatalysts based on bismuth compounds reported by other investigators. The results (Figure 4) show that bismuth oxo citrate has significantly higher photocatalytic activity than commercial TiO_2. It also shows much higher photocatalytic activity than the photocatalysts based on

Table 1—Comparison of photocatalytic activity of different photocatalysts based on bismuth compounds.

Photocatalyst	Dye	c_{dye}/c_{phot} (mol mg^{-1})	Time (min)	RE (%)	k_{app} (min^{-1})	Ref
Dy doped Bi_2O_3	MO	$3.05 \cdot 10^{-5}$	60	31.5	/	(Li et al., 2013)
$Bi_6O_6(OH)_3(NO_3)_3 \cdot 1.5H_2O$	MG	$5.48 \cdot 10^{-5}$	120	74.0	/	(Xie, Wang, Hu, Zheng et al., 2012)
	MO	$6.11 \cdot 10^{-5}$	40	96.0		
Bi_2O_3/H-ZSM-5	RhB	$1.04 \cdot 10^{-5}$	120	95.0	0.0220	(Wang, Hui et al., 2014)
$MoS_2/Bi_2O_2CO_3$	RhB	$2.09 \cdot 10^{-5}$	90	98.0	0.0298	(Wang, Yun et al., 2014)
Pd doped Bi_2O_3	MO	$3.05 \cdot 10^{-5}$	120	30.0	/	(Zhong et al., 2014)
$ZrO_2/Bi_6O_6(OH)_3(NO_3)_3 \cdot 1.5H_2O$	MG	$5.48 \cdot 10^{-5}$	40	96.0	/	(Xie, Wang, Hu, Zhu et al., 2012)
Bismuth oxo citrate	RB19	$7.98 \cdot 10^{-5}$	15	90.5	0.25	this work

Allen Press, Inc. ■ 5 April 2018 ■ 6:21 pm ■ Customer MS#WER-D-17-00201
//titan/Production/w/waer/live_jobs/waer-90/waer-90-07/waer-90-07-07/layouts/waer-90-07-07.3d

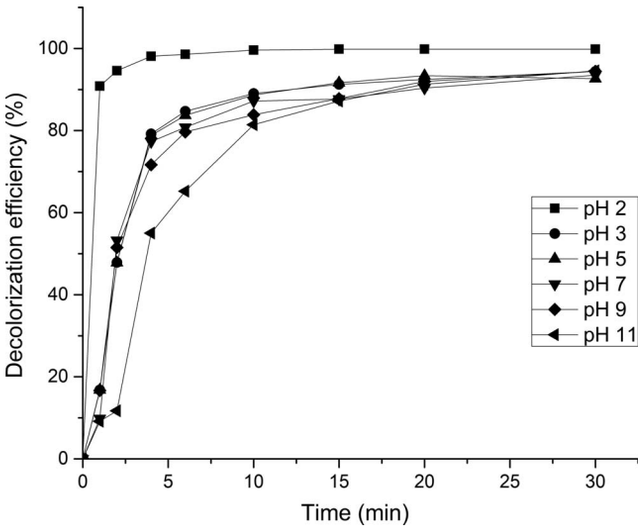

Figure 5—Effect of pH on the photocatalyst decolorization efficiency. c_{RB19} 25 mg dm^{-3}, $c_{photocatalyst}$ 500 mg dm^{-3}, UV light intensity 1950 μW cm^{-2}, temperature 20.0 ± 0.5 °C.

bismuth compounds reported by other investigators (Table 1): bismuth oxo citrate can decolorize much higher dye concentration in the same period of time. Furthermore, the ratio of dye concentration and photocatalyst dose is higher for bismuth oxo citrate in comparison with other photocatalysts, which means that if the same amount of photocatalyst is used, bismuth oxo citrate will degrade much higher amount of dye. Also, the first-order rate constant is significantly higher in the photocatalytic treatment with bismuth oxo citrate as photocatalyst (Li et al., 2013; Wang, Hui et al., 2014; Wang, Yun et al., 2014; Xie, Wang, Hu, Zheng et al., 2012; Xie, Wang, Hu, Zhu et al., 2012; Zhong et al., 2014). Preliminary studies have shown that bismuth oxo citrate photocatalyst can also successfully degrade other textile dyes, such as RO4 and RO16 (Figure S3). The rate of photodegradation is similar for all three dyes. The influence of different parameters on the photocatalytic process was investigated by using RB19 as model pollutant and the results are given below.

Effect of the Initial pH on the Photocatalytic Performance. The pH of contaminated water can have different values. Therefore, it is very important to study the effect of initial pH on the photocatalytic decolorization of dye. Photocatalytic activity was investigated at various initial pH values (2, 3, 5, 7, 9, and 11), using fixed dye concentration and photocatalyst dose. The decolorization of dye as a function of the initial pH is shown in Figure 5.

From Figure 5, it can be observed that decolorization efficiency is the largest in acidic medium (pH 2). With the increase of initial pH from 2 to 11, decolorization efficiency decreases. The decolorization efficiency rapidly decreases between initial pH 2 and 3, while for initial pH $\geq$ 3, decolorization efficiency slightly decreases. Such a dependence of pH on the decolorization efficiency can be explained by the dye adsorption capability of photocatalyst at the different pH values. To study this effect, dye adsorption on the photocatalyst surface was investigated at different pH values (results not shown). Adsorption was negligible at the pH $\geq$ 3, while it is significantly higher at pH 2 (about 6 mg g^{-1}). This can be explained by the surface charge according to pI value. At pH 2, photocatalyst surface is positively charged (pI is 3.17) and, because RB19 is anionic dye and thus negatively charged, the adsorption at pH $<$ 3 is favored because of the electrostatic attraction between the dye molecules and photocatalyst surface. Thus, the decolorization efficiency is highest at low pH values, because electrostatic attraction and sorption of RB19 accelerates the photocatalytic process.

Effect of the Photocatalyst Dose on the Photocatalytic Performance. The photocatalyst dose is one of the main parameters for the degradation of pollutants with the photocatalytic process. To determine the optimal photocatalyst dose, a series of experiments was conducted by varying the initial photocatalyst dose (50, 100, 250, 500, 800, and 1200 mg dm^{-3}) at native pH and fixed initial dye concentration. The results are shown in Figure 6.

An increase in photocatalyst dose from 50 to 250 mg dm^{-3} increases the decolorization rate rapidly. With further increase of photocatalyst dose from 250 to 1200 mg dm^{-3} decolorization rate decreases. The total active surface area increases with the increasing of photocatalyst dosage, hence decolorization is faster. However, higher photocatalyst dose leads to an increase in turbidity of the solution. This affects the reduction of UV light penetration through the solution as a result of increased light scattering by photocatalyst particles and, therefore, decolorization efficiency decreases (Daneshvar et al., 2004). Thus, it can be concluded that higher photocatalyst dose may not be useful. Hence, the optimal photocatalyst concentration is 250 mg dm^{-3}.

Effect of the Initial Dye Concentration on the Photocatalytic Performance. The degradation rate of the pollutant is of crucial importance for the water treatment. Thus, the effect of initial dye concentration on the decolorization efficiency was investigated by varying its value from 10 to 100 mg L^{-1} at constant catalyst loading and pH value of the solution. The results are shown in Figure 7.

As shown in Figure 7, the decolorization efficiency decreases with increasing dye concentration. At higher dye concentrations, production of •OH radicals is reduced due to adsorption of dye molecules on the active sites of the photocatalyst surface. Also, as the dye concentration increases, solution becomes less transparent to UV light because dye molecules may absorb a significant amount of UV light. Thus, the path length of photons entering the solution decreases and less number of photons is available to reach the photocatalyst surface (Ćurković et al., 2014; Kansal et al., 2007). This is the reason for the decreases of the photocatalytic reaction rate with increasing dye concentration.

Reusability of the Photocatalyst. Reusability of the synthesized photocatalyst is very important for its potential practical application. Therefore, photocatalytic process of the

Allen Press, Inc. ■ 5 April 2018 ■ 6:22 pm ■ Customer MS#WER-D-17-00201
//titan/Production/w/waer/live_jobs/waer-90/waer-90-07/waer-90-07-07/layouts/waer-90-07-07.3d

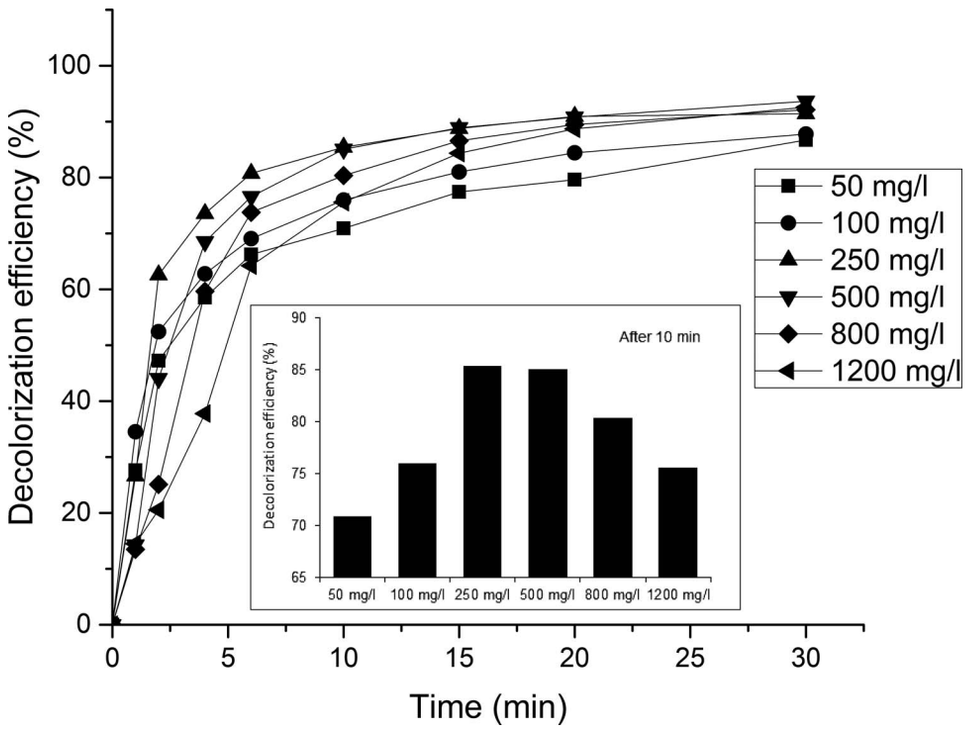

Figure 6—Effect of initial photocatalyst dose on the decolorization efficiency of RB19. c_{RB19} 25 mg dm^{-3}, UV light intensity 1950 μW cm^{-2}, temperature 20.0 ± 0.5 °C, pH native (4.7).

degradation of RB19 was done in five cycles with the same photocatalyst. The photocatalyst was recycled after treatment by centrifugation, and used for the next treatment. After the fifth cycle, bismuth oxo citrate kept almost the same photocatalytic activity (Figure 8). This implies that bismuth oxo citrate has good stability and that it is reusable as photocatalyst.

Photocatalysis Kinetics. *Langmuir–Hinshelwood Model.* The Langmuir–Hinshelwood (L–H) model has been successfully used to describe the heterogeneous reaction occurring at a solid–liquid interface (Hamad et al., 2016; Thu and Juang, 2015). According to the L–H model, the rate of a unimolecular surface reaction, r, is proportional to surface coverage and will follow

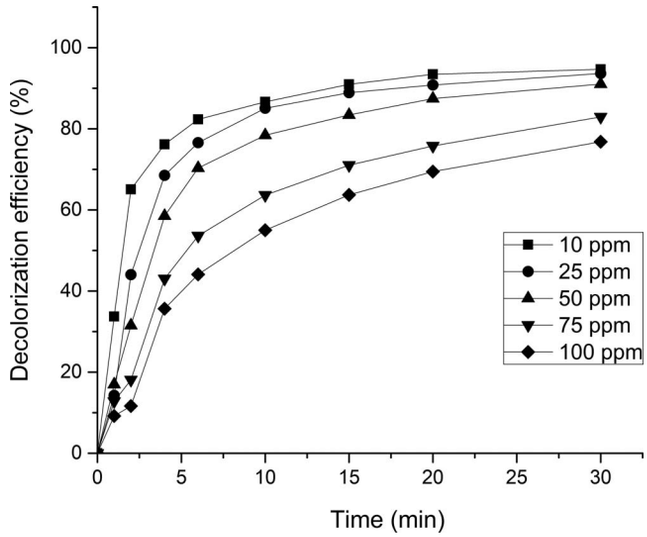

Figure 7—Effect of initial dye concentration on the decolorization efficiency of RB19. $c_{photocatalyst}$ 500 mg dm^{-3}, UV light intensity 1950 μW cm^{-2}, temperature 20.0 ± 0.5 °C, pH native (4.7).

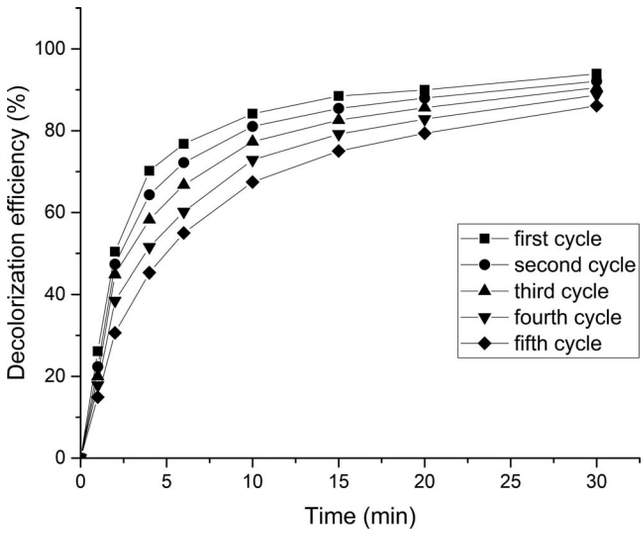

Figure 8—Reusability of the photocatalyst in five cycles for the decolorization of RB19. c_{RB19} 25 mg dm^{-3}, UV light intensity 1950 μW cm^{-2}, temperature 20.0 ± 0.5 °C, pH native (4.7).

Allen Press, Inc. ■ 5 April 2018 ■ 6:22 pm ■ Customer MS#WER-D-17-00201
//titan/Production/w/waer/live_jobs/waer-90/waer-90-07/waer-90-07-07/layouts/waer-90-07-07.3d

Table 2—Kinetic parameters for photocatalytic decolorization of RB19.

Model	Constant	c_{RB19} 10 mg dm^{-3}	c_{RB19} 25 mg dm^{-3}	c_{RB19} 50 mg dm^{-3}	c_{RB19} 75 mg dm^{-3}	c_{RB19} 100 mg dm^{-3}
	q_{exp}	19.45	49.83	92.86	124.04	149.93
Langmuir–Hinshelwood	k_{app}	0.40	0.25	0.17	0.12	0.09
	R^2	0.958	0.981	0.989	0.984	0.975
Pseudo-first	q_e	18.62	48.71	90.14	119.92	148.83
	k_1	0.52	0.30	0.24	0.17	0.13
	R^2	0.991	0.992	0.994	0.993	0.992
Pseudo-second	q_e	20.62	56.64	107.06	149.80	193.25
	k_1	0.70	0.35	0.27	0.17	0.12
	R^2	0.983	0.971	0.978	0.981	0.979
Chrastil	q_e	18.73	47.76	89.22	119.63	147.20
	k_c	0.89	0.88	0.57	0.34	0.29
	n	0.86	1.05	1.07	1.02	1.06
	R^2	0.982	0.989	0.994	0.987	0.985

eqs 2 and 3, when the reactant is more strongly adsorbed on the surface than the products:

$$r = -\frac{dc}{dt} = \frac{k_r K c}{1 + Kc} \tag{2}$$

$$\frac{1}{r} = \frac{1}{k_r K c} + \frac{1}{k_r} \tag{3}$$

where r (mg dm^{-3} min^{-1}) is the rate of photocatalytic degradation of RB19, c (mg dm^{-3}) is the concentration of RB19, and t (min) is the reaction time. K (dm^{-3} min^{-1}) represents the equilibrium constant for adsorption of RB19 on to illuminated photocatalyst and k_r (mg dm^{-3} min^{-1}) reflects the reaction rate constant at maximum coverage under the given experimental conditions.

For low substrate concentrations (approximately $<10^{-3}$ mol dm^{-3} where $Kc << 1$) and when adsorption is relatively weak eq 2 can be simplified to a pseudo-first order kinetic relationship as shown in eq 4 (Thu and Juang, 2015):

$$r = -\frac{dc}{dt} = k_r K c = k_{app} c \tag{4}$$

where c is the RB19 concentration at time t, and k_{app} (min^{-1}) the apparent first-order rate constant. The integrated form of eq 4 in linear and nonlinear form is

$$\ln\left(\frac{c_t}{c_0}\right) = -k_{app} t \tag{5}$$

$$\frac{c_t}{c_0} = e^{-k_{app} t} \tag{6}$$

where c_0 is the RB19 concentration at the initial time.

A plot of c_0/c versus irradiation time t is shown in Figure S4. The apparent first-order rate constant k_{app} was determined by a nonlinear regression analysis using software Origin 2016 (OriginLab Corp.) and results are presented in Table 2. The determination coefficients are high for all initial concentrations of dye. Therefore, it can be concluded that the photocatalytic process follows the pseudo-first order kinetics model. The rate constant decreases with increasing dye concentration, which means that the decolorization process is slower for higher initial dye concentrations.

The applicability of L–H model was confirmed by linear plot (Figure S5) obtained by reciprocal of reaction rate ($1/r$) against reciprocal of the initial concentration of RB19 ($1/c_0$). The obtained values for the equilibrium constant for adsorption (K) and the reaction rate constant (k_r) are 0.06 dm^{-3} min^{-1} and 10.80 mg dm^{-3} min^{-1}, respectively. Determination coefficient R^2 is 0.995. Because the reaction rate constant of the photocatalytic reaction is large, and the adsorption constant is small, adsorption is a limiting factor of the photocatalytic reaction and thus sorption kinetics models can be applied on this process.

Pseudo-First and Pseudo-Second Order Model. To investigate kinetics of the photocatalytic process, the applicability of the pseudo-first and pseudo-second order model was tested. Pseudo-first (eq 7) and pseudo-second (eq 8) order nonlinear equations were used to fit the experimental kinetics data.

$$q_t = q_e(1 - e^{-k_1 t}) \tag{7}$$

$$q_t = \frac{k_2 q_e^2 t}{1 + k_2 q_e t} \tag{8}$$

where q_t is the concentration of decolorized dye after irradiation time t (mg g^{-1}), q_e is the concentration of decolorized dye at equilibrium state (mg g^{-1}), k_1 (min^{-1}) and k_2 (g mg^{-1} min^{-1}) are the rate constants for the pseudo-first and pseudo-second order kinetic equations, respectively (Azizian, 2004). The model parameters k_1, k_2, and q_e were determined by a nonlinear regression analysis and results of fitting the experimental data are presented in Table 2.

To determine the applicability of pseudo-first and pseudo-second order models in different conditions, fittings were done for all initial concentrations of dye. The determination coefficients are high for both of the models, but they are slightly higher for the pseudo-first order model (Table 2). The calculated q_e (mg g^{-1}) values from the pseudo-first order model are in better agreement with the experimental ones. Therefore, it can be concluded that the photocatalytic process follows the pseudo-first order kinetics model. With the increase in initial color

Allen Press, Inc. ■ 5 April 2018 ■ 6:22 pm ■ Customer MS#WER-D-17-00201
//titan/Production/w/waer/live_jobs/waer-90/waer-90-07/waer-90-07-07/layouts/waer-90-07-07.3d

concentration, the rate constant decreases, so the decolorization process is slower for higher dye concentrations.

Chrastil Diffusion Model. The Chrastil diffusion model is used for description of the kinetics of the heterogeneous and diffusion limited systems and can be expressed by the following equation (Chrastil, 1990):

$$q_t = q_e(1 - e^{-k_c q_0 t})^n \quad (9)$$

where q_t is the concentration of decolorized dye after irradiation time t (mg g^{-1}), q_e is the concentration of decolorized dye at equilibrium state (mg g^{-1}), k_c is a rate constant (dm^3 g^{-1} min^{-1}), q_0 is the concentration of photocatalyst (g dm^{-3}), and n is a heterogeneous structural diffusion resistance constant with reaction order characteristics. From the value of constant n, diffusion characteristic and order of reaction can be determined. If reactions are diffusion limited, then: $n < 1$, and in the case when diffusion resistance is small, then: $n \geq 1$. For the first-order reactions, $n = 1$, second and higher order reactions have $n < 1$, and consecutive reactions have $n > 1$ (Chrastil, 1988).

The photocatalytic degradation of RB19 with bismuth oxo citrate was done in a heterogeneous system where diffusion can have influence. To investigate influence of the diffusion resistance on the photocatalytic process, the Chrastil model was applied. Parameters q_e, k_c, and n were determined by nonlinear fitting of the experimental data for different initial concentrations of dye and results are presented in Table 2. For the dye concentrations: 25, 50, 75, and 100 mg dm^{-3}, constant n is approximately 1, which means that diffusion resistance is small and reaction follows the pseudo-first order kinetics. For the lowest dye concentration (10 mg dm^{-3}), n was 0.86, which indicates that diffusion have some influence on the process, but this influence is relatively small, since n is not significantly lower than 1. Theoretically, calculated q_e values by this model are close to experimental values. With increasing the initial dye concentration, the rate constant k_c decreases, because of the reasons described before in the paper. The determination coefficients are higher than 0.98, which is high enought to assume that the Chrastil model can be applied for the described reactions.

The results obtained by the Chrastil model are in good agreement with the L–H model for the reaction with the pseudo-first order kinetics, which confirms applicability of these models on photocatalytic decolorization of RB19.

Conclusion

A new photocatalyst based on bismuth oxo citrate was successfully synthesized by the facile precipitation method. The photocatalyst was characterized by different methods and results showed that obtained material has the following structure: $BiOC_6H_7O_7 \cdot H_2O$. A relatively high surface area (8.92 m^2 g^{-1}) and mesoporous structure of material affects the high photocatalytic efficiency for decolorization of RB19. The pI value of the photocatalyst is 3.17 and its surface is positively charged at lower pH values. Because of that chemical sorption of RB19 occurs at pH lower than 3 and photocatalytic efficiency is higher at pH < 3. The optimal pH of the photocatalytic process is 2. The decolorization of RB19 is directly related to the dose of photocatalyst in the suspension, and the optimal photocatalyst dose is 250 mg dm^{-3}. The initial dye concentration affects the dye decolorization rate: an increase of the initial dye concentration leads to decrease of the reaction rate constants. The photocatalytic process follows L–H model simplified to the pseudo-first order kinetic model. From the Chrastil model it can be seen that diffusion has no influence on the photocatalysis process (except for the lowest dye concentration, where a relatively small diffusion resistance occurs). High efficiency, good reusability, facile synthesis, low cost and eco-friendly starting materials makes the new photocatalyst a promising means for the removal of reactive dyes from water.

Supplementary Materials

The Supplementary Materials are found in the online version of this article.

Acknowledgment

The authors would like to acknowledge for financial support to the Ministry of Education, Science and Technological Development of the Republic of Serbia (Grant No. TR34008).

Submitted for publication Month , ; accepted for publication Month , .

References

Afonina, L. I.; Naydenko, E. S.; Yukhin, Y. M.; Danilova, L. E. (2009) Synthesis of High-Pure Bismuth Citrate Using the Solid-Liquid Reactions. *Chem. Sustain. Dev.*, **17** (3), 235–241.

Anandan, S.; Lee, G.-J.; Chen, P.-K.; Fan, C.; Wu, J. J. (2010) Removal of Orange II Dye in Water by Visible Light Assisted Photocatalytic Ozonation Using Bi_2O_3 and Au/Bi_2O_3 Nanorods. *Ind. Eng. Chem. Res.*, **49** (20), 9729–9737.

Azizian, S. (2004) Kinetic Models of Sorption: A Theoretical Analysis. *J. Colloid Interface Sci.*, **276** (1), 47–52.

Barrett, E. P.; Joyner, L. G.; Halenda, P. P. (1951) The Determination of Pore Volume and Area Distributions in Porous Substances. I. Computations from Nitrogen Isotherms. *J. Am. Chem. Soc.*, **73** (1), 373–380.

Brunauer, S.; Emmett, P. H.; Teller, E. (1938) Adsorption of Gases in Multimolecular Layers. *J. Am. Chem. Soc.*, **60** (2), 309–319.

Chen, C.; Ma, W.; Zhao, J. (2010) Semiconductor-Mediated Photodegradation of Pollutants Under Visible-Light Irradiation. *Chem. Soc. Rev.*, **39** (11), 4206–4219.

Chong, M. N.; Jin, B.; Chow, C. W. K.; Saint, C. (2010) Recent Developments in Photocatalytic Water Treatment Technology: A Review. *Water Res.*, **44** (10), 2997–3027.

Chrastil, J. (1990) Adsorption of Direct Dyes on Cotton: Kinetics of Dyeing from Finite Baths Based on New Information. *Text. Res. J.*, **60** (7), 413–416.

Chrastil, J. (1988) Determination of the First Order Consecutive Reaction Rate Constants from Final Product. *Comput. Chem.*, **12** (4), 289–292.

Ćurković, L.; Ljubas, D.; Šegota, S.; Bačić, I. (2014) Photocatalytic Degradation of Lissamine Green B Dye by Using Nanostructured Sol-Gel TiO_2 Films. *J. Alloys Compd.*, **604**, 309–316.

Daneshvar, N.; Salari, D.; Khataee, A. (2004) Photocatalytic Degradation of Azo Dye Acid Red 14 in Water on ZnO as an Alternative Catalyst to TiO_2. *J. Photochem. Photobiol. A Chem.*, **162** (2–3), 317–322.

Evseenko, V. I.; Logutenko, O. A.; Yukhin, Y. M. (2004) Synthesis of High-Purity Bismuth (III) Tartratahydrotartrate Trihydrate. *Chem. Sustain. Dev.*, **12** (1), 39–45.

Fruth, V.; Popa, M.; Berger, D.; Ionica, C. M.; Jitianu, M. (2004) Phases Investigation in the Antimony Doped Bi_2O_3 System. *J. Eur. Ceram. Soc.*, **24**, 1295–1299.

Gyliene, O.; Nivinskiene, O.; Pakštas, V. (2007) Use of Metallic Iron for Decontamination of Solution Containing Ni(II)-Citrate. *Polish J. Environ. Stud.*, **16** (3), 397–402.

Hamad, H. A.; Sadik, W. A.; El-latif, M. M. A.; Kashyout, A. B.; Feteha, M. Y. (2016) Photocatalytic Parameters and Kinetic Study for Degradation of Dichlorophenol-Indophenol (DCPIP) Dye Using Highly Active Mesoporous TiO_2 Nanoparticles. *J. Environ. Sci.*, **43**, 26–39.

Irmawati, R.; Nasriah, M. N. N.; Taufiq-Yap, Y. H.; Hamid, S. B. A. (2004) Characterization of Bismuth Oxide Catalysts Prepared from Bismuth Trinitrate Pentahydrate: Influence of Bismuth Concentration. *Catal. Today*, **93–95**, 701–709.

Kamat, P. V. (1993) Photochemistry on Nonreactive and Reactive (Semiconductor) Surfaces. *Chem. Rev.*, **93** (1), 267–300.

Kansal, S. K.; Singh, M.; Sud, D. (2007) Studies on Photodegradation of Two Commercial Dyes in Aqueous Phase Using Different Photocatalysts. *J. Hazard. Mater.*, **141** (3), 581–590.

Lakshmanan, B. (1968) Infrared Absorption Spectrum of Sodium Citrate. *J. Indian Inst. Sci.*, **39** (1954), Suppl:108-120.

Li, J. Z.; Zhong, J. B.; Zeng, J.; Feng, F. M.; He, J. J. (2013) Improved Photocatalytic Activity of Dysprosium-Doped Bi_2O_3 Prepared by Sol–Gel Method. *Mater. Sci. Semicond. Process.*, **16** (2), 379–384.

Li, K.-L.; Lee, W. W.; Lu, C.-S.; Dai, Y.-M.; Chou, S.-Y.; Chen, H.-L.; Lin, H.-P.; Chen, C.-C. (2014) Synthesis of BiOBr, Bi_3O_4Br, and $Bi_{12}O_{17}Br_2$ by Controlled Hydrothermal Method and Their Photocatalytic Properties. *J. Taiwan Inst. Chem. Eng.*, **45** (5), 2688–2697.

Liang, L.; Cao, J.; Lin, H.; Guo, X.; Zhang, M.; Chen, S. (2016) Enhancing Visible Light Photocatalytic and Photocharge Separation of $(BiO)_2CO_3$ Plate Via Dramatic I- Ions Doping Effect. *Mater. Res. Bull.*, **80**, 329–336.

Liu, S.; Tu, Y.; Dai, G. (2014) The Effects of Citrate Ion on Morphology and Photocatalytic Activity of Flower-Like $Bi_2O_2CO_3$. *Ceram. Int.*, **40** (1), 2343–2348.

Mahmood, T.; Saddique, M. T.; Naeem, A.; Westerhoff, P.; Mustafa, S.; Alum, A. (2011) Comparison of Different Methods for the Point of Zero Charge Determination of NiO. *Ind. Eng. Chem. Res.*, **50** (17), 10017–10023.

Mitrović, J.; Radović, M.; Bojić, D.; Anbelković, T.; Purenović, M.; Bojić, A. (2012) Decolorization of the Textile Azo Dye Reactive Orange 16 by the UV/H_2O_2 Process. *J. Serbian Chem. Soc.*, **77** (4), 465–481.

Naydenko, E. S.; Yukhin, Y. M.; Afonina, L. I. (2012) Preparation of Bismuth (III) Citrate via Precipitation from the Solutions of Mineral Acids. *Chem. Sustain. Dev.*, **20**, 189–196.

Prekajski, M.; Kremenović, A.; Babić, B.; Rosić, M.; Matović, B.; Radosavljević-Mihajlović, A.; Radović, M. (2010) Room-Temperature Synthesis of Nanometric α-Bi_2O_3. *Mater. Lett.*, **64** (20), 2247–2250.

Saison, T.; Chemin, N.; Chanéac, C.; Durupthy, O.; Ruaux, V.; Mariey, L.; Maugé, F.; Beaunier, P.; Jolivet, J.-P. (2011) Bi_2O_3, $BiVO_4$, and Bi_2WO_6 : Impact of Surface Properties on Photocatalytic Activity under Visible Light. *J. Phys. Chem. C*, **115** (13), 5657–5666.

Shang, M.; Wang, W.; Zhang, L.; Sun, S.; Wang, L.; Zhou, L. (2009) 3D Bi_2WO_6/TiO_2 Hierarchical Heterostructure: Controllable Synthesis and Enhanced Visible Photocatalytic Degradation Performances. *J. Phys. Chem. C*, **113** (33), 14727–14731.

Taqa, A. A. (2011) Preparation of Potassium Dicitro Bismuthate Complex as Antigastric Ulcer. *Rafidain J. Sci.*, **22** (2), 39–49.

Thottoli, A. K. and Unni, A. K. A. (2013) Effect of Trisodium Citrate Concentration on the Particle Growth of ZnS Nanoparticles. *J. Nanostructure Chem.*, **3** (1), 56.

Thu, A.; Juang, R. (2015) Photocatalytic Degradation of P-Chlorophenol by Hybrid H_2O_2 and TiO_2 In Aqueous Suspensions Under UV Irradiation. *J. Environ. Manage.*, **147**, 271–277.

Wang, K.; Shao, C.; Li, X.; Miao, F.; Lu, N. (2016) Room Temperature Immobilized BiOI Nanosheets on Flexible Electrospun Polyacrylonitrile Nanofibers with High Visible-Light Photocatalytic Activity. *J. Sol-Gel Sci. Technol.*, **80**, 783–792.

Wang, Q.; Hui, J.; Yang, L.; Huang, H.; Cai, Y.; Yin, S.; Ding, Y. (2014) Enhanced Photocatalytic Performance of Bi_2O_3/H-ZSM-5 Composite for Rhodamine B Degradation Under UV Light Irradiation. *Appl. Surf. Sci.*, **289**, 224–229.

Wang, Q.; Yun, G.; Bai, Y.; An, N.; Lian, J.; Huang, H.; Su, B. (2014) Photodegradation of Rhodamine B with MoS_2/$Bi_2O_2CO_3$ Composites Under UV Light Irradiation. *Appl. Surf. Sci.*, **313**, 537–544.

Wu, Y. C.; Chaing, Y. C.; Huang, C. Y.; Wang, S. F.; Yang, H. Y. (2013) Morphology-Controllable Bi_2O_3 Crystals Through an Aqueous Precipitation Method and Their Photocatalytic Performance. *Dye. Pigment.*, **98** (1), 25–30.

Xie, L.; Wang, J.; Hu, Y.; Zheng, Z.; Weng, S.; Liu, P.; Shi, X.; Wang, D. (2012) Template-Free Microwave-Assisted Hydrothermal Synthesis and Photocatalytic Performance of $Bi_6O_6(OH)_3(NO_3)_3$·1.5H_2O Nanosheets. *Mater. Chem. Phys.*, **136** (2–3), 309–312.

Xie, L.; Wang, J.; Hu, Y.; Zhu, S.; Zheng, Z.; Weng, S.; Liu, P. (2012) ZrO_2-Incorporated $Bi_6O_6(OH)_3(NO_3)_3$·1.5H_2O with Superior Photocatalytic Activity for Degradation of Malachite Green. *RSC Adv.*, **2** (26), 9881–9886.

Xu, F.; Tan, W.; Liu, H.; Li, D.; Li, Y.; Wang, M. (2016) Immobilization of PDMS-SiO_2-TiO_2 Composite for the Photocatalytic Degradation of Dye AO-7. *Water Sci. Technol.*, **74** (7), 1680–1688.

Xu, Z.; Zhang, M.; Wu, J.; Liang, J.; Zhou, L.; Lü, B. (2013) Visible Light-Degradation of Azo Dye Methyl Orange Using TiO_2/β-FeOOH as a Heterogeneous Photo-Fenton-Like Catalyst. *Water Sci. Technol.*, **68** (10), 2178–2185.

Yang, N.; Sun, H. (2007) Biocoordination Chemistry of Bismuth: Recent Advances. *Coord. Chem. Rev.*, **251** (17–20), 2354–2366.

Zhong, J.; Li, J.; Feng, F.; Fan, G.; Zeng, J.; Huang, S.; Hu, W.; Li, M. (2014) Improved Photocatalytic Decolorization of Methyl Orange over Pd-doped Bi_2O_3. *Environ. Prog. Sustain. Energy*, **33** (4), 1229–1234.

Allen Press, Inc. ■ 5 April 2018 ■ 6:22 pm ■ Customer MS#WER-D-17-00201
//titan/Production/w/waer/live_jobs/waer-90/waer-90-07/waer-90-07-07/layouts/waer-90-07-07.3d

Queries for waer-90-07-07

This manuscript/text has been typeset from the submitted material. Please check this proof carefully to make sure there have been no font conversion errors or inadvertent formatting errors. Allen Press.